MANCHESTER 1824
The University of Manchester

The University of Manchester Research

Ambipolar SnOx Thin-Film Transistors Achieved at High Sputtering Power

DOI:
10.1063/1.5022875

Document Version
Accepted author manuscript

Link to publication record in Manchester Research Explorer

Citation for published version (APA):
Yunpeng Li, Jia Yang, Qu, Y., Zhang, J., Zhou, L., Yang, Z., Lin, Z., Qingpu Wang, Song, A., & Qian Xin (2018). Ambipolar SnOx Thin-Film Transistors Achieved at High Sputtering Power. *Applied Physics Letters*, *112*, [182102]. https://doi.org/10.1063/1.5022875

Published in:
Applied Physics Letters

Citing this paper
Please note that where the full-text provided on Manchester Research Explorer is the Author Accepted Manuscript or Proof version this may differ from the final Published version. If citing, it is advised that you check and use the publisher's definitive version.

General rights
Copyright and moral rights for the publications made accessible in the Research Explorer are retained by the authors and/or other copyright owners and it is a condition of accessing publications that users recognise and abide by the legal requirements associated with these rights.

Takedown policy
If you believe that this document breaches copyright please refer to the University of Manchester's Takedown Procedures [http://man.ac.uk/04Y6Bo] or contact uml.scholarlycommunications@manchester.ac.uk providing relevant details, so we can investigate your claim.

Download date:27. Aug. 2022

Ambipolar SnO_x Thin-Film Transistors Achieved at High Sputtering Power

Yunpeng Li[1], Jia Yang[1], Yunxiu Qu[1], Jiawei Zhang[2], Li Zhou[1], Zaixing Yang[1], Zhaojun Lin[1], Qingpu Wang[1], Aimin Song[1,2,a)], and Qian Xin[1,a)]

[1]*Center of Nanoelectronics, State Key Laboratory of Crystal Materials, and School of Microelectronics, Shandong University, Jinan 250100, China*

[2]*School of Electrical and Electronic Engineering, University of Manchester, Manchester M13 9PL, United Kingdom*

SnO is the only oxide semiconductor to date that has exhibited ambipolar behavior in thin-film transistors (TFTs). In this work, ambipolar behavior was observed in SnO_x TFTs fabricated at a high sputtering power of 200 W and post-annealed at 150-250 ^{o}C in ambient air. X-ray-diffraction patterns show polycrystallisation of SnO and Sn in the annealed SnO_x films. Scanning-electron-microscopy images revealed that microgrooves occurred after the films were annealed. Clusters subsequently segregated along the microgrooves, and our experiments suggested that they are most likely Sn clusters. Atomic-force-microscopy images indicated an abrupt increase in film roughness due to the cluster segregations. An important implication of this work is that excess Sn in the film, which has been generally thought to be detrimental to the film quality, may promote the ambipolar conduction when it is segregated from the film to enhance the stoichiometric balance.

Oxide semiconductors are highly attractive especially for the new generation flexible and wearable electronics due to their low cost, low deposition temperatures, high carrier mobilities (1~100 cm^2/Vs), good transparency in the visible-light region, and ease of large-area manufacturing.[1-4] To date, n-type oxides, such as ZnO and InGaZnO, are highly developed and even commercialized. On the contrary, the development of their p-type counterparts is far behind, and ambipolar oxides that can exhibit both n- and p-type conduction are even rarer.[5-9] To fabricate all-oxide-based complementary-metal-oxide-semiconductor (CMOS) -like circuits, it is essential to develop high-performance p-type or ambipolar oxide semiconductors. In particular, ambipolar semiconductors can significantly simplify the fabrication process of

a) Authors to whom correspondence should be addressed. Electronic mail: A.Song@manchester.ac.uk and xinq@sdu.edu.cn

CMOS circuits and allow more compact CMOS architectures.[9] Hence, extraordinary efforts have been made to develop ambipolar semiconductors and related thin-film-transistors (TFTs). Up to now, nanocrystalline silicon, organic semiconductors, and carbon nanotubes have been found capable of operating in ambipolar mode, due to either a small bandgap or low density of subgap states.[8-10] Recently, tin monoxide (SnO) has been found capable of operating in ambipolar mode, and this is the only oxide semiconductor capable of conducting both electrons and holes effectively in a TFT.[11,12] Voltage gains of CMOS-like inverters based on such ambipolar SnO TFTs have been shown to be higher than 100.[6]

Ambipolar behavior is generally difficult to achieve in most oxide TFTs because of their typically large fundamental bandgaps and a high density of subgap states.[13-15] SnO is regarded as the most promising p-type oxide among the limited number of p-type oxides discovered so far.[12] The ambipolar behavior of SnO has been thought to be due to its low electron effective mass (~0.4 m_0), low hole effective mass (~0.6 m_0), and small fundamental bandgap (~0.7 eV).[11,16,17] However, the density of subgap states in some p-type SnO TFTs extracted by temperature-dependent field-effect results can be higher than 10^{19} $eV^{-1}cm^{-3}$,[15,18] which supresses the ambipolar behavior. In 2011, Nomura *et al.* fabricated the first SnO-based ambipolar TFT.[11] Subsequently, Cao *et al.* fabricated ambipolar SnO TFT with balanced electron and hole mobilities.[5,6] In 2016, Chen *et al.* demonstrated controllability of ambipolar conduction in SnO_x TFTs by oxygen plasma treatment.[19] In 2017, Kim *et al.* observed clear ambipolar operation in TFTs based on atomic-layer-deposited SnO films as the active layer.[20] Despite these processes, studies on how the ambipolar conduction and associated microstructures change in SnO film under thermal treatment are still limited.

In this work, ambipolar SnO_x channel layers were achieved by using a high sputtering power of 200 W and post-annealing in ambient air without passivation. The ambipolar behavior appeared when microgrooves occurred and nanoclusters segregated along the microgrooves in the SnO_x film. Our study indicates that the appearance of ambipolar behavior is a result of both a reduction of density of subgap states by Sn interstitials (Sn_i) and suppression of interfacial trap states because of the segregation of Sn clusters.

The schematic diagram of our SnO_x TFTs is shown in Fig. 1(a). Heavily doped p-type silicon wafers were used as both substrates and gate electrodes. 300-nm-thick thermally grown

SiO_2 was employed as the gate dielectrics. SnO_x active layers were deposited onto the SiO_2 surfaces using reactive radio-frequency magnetron sputtering method with a deposition power of 200 W from a 3 inches Sn target (99.99% purity). The Ar/O_2 mixture atmosphere was fixed at a ratio of 23/3 (sccm/sccm). The working pressure during the sputtering process was ~4.8 mTorr. The substrate temperature was kept at 100 ^oC. The thickness of the SnO_x layers was 27 nm. 50-nm-thick Pd source and drain electrodes were deposited by electron-beam evaporation, and the length and width of the active channel were 60 and 2000 μm, respectively. Finally, the devices were annealed at 150, 175, 200, 225, and 250 ^oC for 1 hour in ambient air step by step.

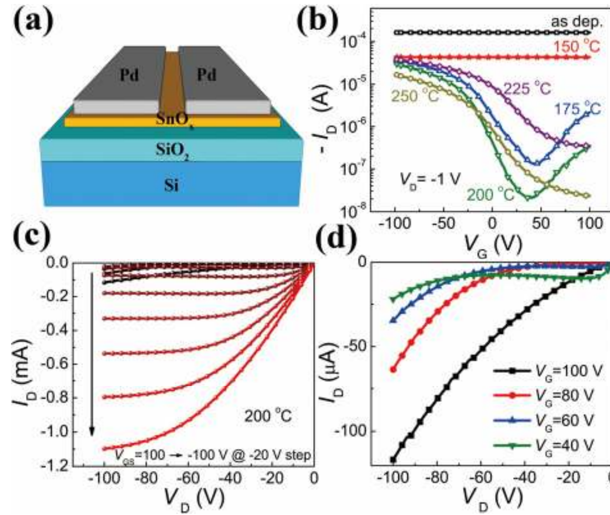

FIG. 1. (a) Schematic diagram of SnO_x TFT, (b) transfer curves of the as-deposited and annealed (at 150, 175, 200, 225, and 250 ^oC) SnO_x TFTs, (c) output curves of the TFT post-annealed at 200 ^oC , (d) a zoomed view of figure (c) when V_G = 40-100 V.

Figure 1(b) shows the transfer curves of the TFT annealed at different temperatures. The channel layer of the as-deposited TFT was too conductive to be tuned by gate voltages V_G. The source-drain current, I_D, decreased by ~ 4 times after the TFT was annealed at 150 ^oC in air due to oxidation of excess metallic Sn, but still could not be tuned by gate voltage. After the TFT was annealed at 175 and 200 ^oC, ambipolar behavior was observed. The TFT showed p-type characteristics at negative gate biases and n-type conduction at high positive gate biases (> 40 V). The on/off ratio reached 288 and 1350 for post-annealing temperatures of 175 and 200 ^oC, respectively. As shown in Figs. 1(c) and 1(d), the TFT exhibited pronounced p-type

performance at V_G from +20 to -100 V, and n-type transport was observed at positive V_G from +40 to +100 V. Such ambipolar behavior disappeared with the disappearance of the n-type conduction when the TFT was further annealed at 225 and 250 ^{o}C.

Electrical parameters (on/off ratio I_{on}/I_{off}, electron mobility μ_e, hole mobility μ_h, subthreshold voltage swing SS, and density of subgap trap states D_t) of TFTs annealed at various temperatures were summarized in Table I. The field-effect mobility, μ, was extracted from the linear region of the transfer curve by using[12]

$$I_D = \frac{W}{L} C_{ox} \mu (V_G - V_{th}) V_D, \tag{1}$$

where W and L are the channel width and length, respectively; C_{ox} is the capacitance per unit area of the dielectric; V_{th} is the threshold voltage; and V_D is the drain voltage. As shown in Table I, the n-type SnO_x TFT showed an μ_e of 0.16 and 0.02 $cm^2/(V\cdot s)$ with annealing temperatures of 175 and 200 ^{o}C, respectively. For the p-type SnO_x TFT, the μ_h was 0.97, 0.92, 0.74, and 0.52 $cm^2/(V\cdot s)$ with annealing temperatures of 175, 200, 225, and 250 ^{o}C, respectively.

The SS of the TFT is given by[13]

$$SS = \left[\frac{\partial(\lg I_D)}{\partial(V_G)}\right]^{-1} = \ln(10)\frac{kT}{q}\left(1+\frac{q^2 D_t}{C_{ox}}\right), \tag{2}$$

where k is the Boltzmann constant; T is the temperature; and q is the electron charge. For the p-type SnO_x TFT, SS was 28.36, 18.29, 38.94, and 29.61 V/dec with annealing temperatures of 175, 200, 225, and 250 ^{o}C, respectively. D_t extracted from the transfer curves was 3.42×10^{13}, 2.20×10^{13}, 4.70×10^{13}, and 3.57×10^{13} $cm^{-2}eV^{-1}$ with annealing temperatures of 175, 200, 225, and 250 ^{o}C, respectively.

TABLE I. Electrical parameters of SnO TFTs annealed at 175, 200, 225, and 250 ^{o}C.

T (^{o}C)	I_{on}/I_{off}	μ_e ($cm^2V^{-1}s^{-1}$)	μ_h ($cm^2V^{-1}s^{-1}$)	SS (V/dec)	D_t ($cm^{-2}eV^{-1}$)
175	288	0.16	0.97	28.36	3.42×10^{13}
200	1350	0.02	0.92	18.29	2.20×10^{13}
225	108	-	0.74	38.94	4.70×10^{13}
250	728	-	0.52	29.61	3.57×10^{13}

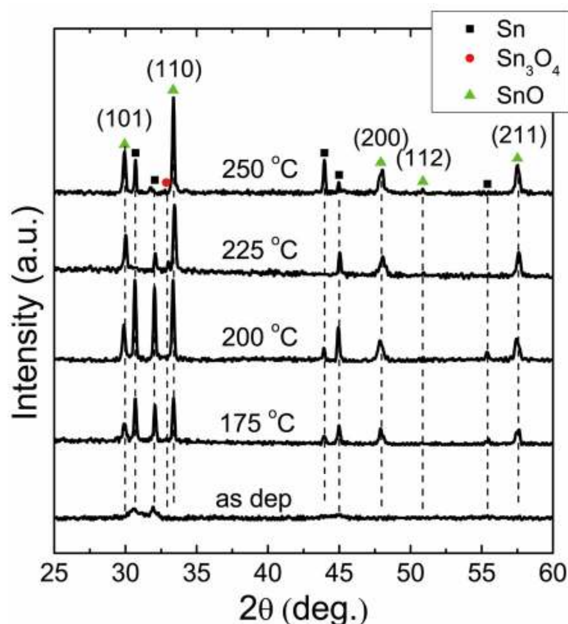

FIG. 2. XRD patterns of one-μm-thick as-deposited and annealed (at 175, 200, 225, and 250 °C) SnO_x films which are sputtered at 200 W.

Figure 2 presents XRD patterns of the as-deposited and annealed one-μm-thick SnO_x films. It indicates that there is crystalized Sn but no crystalized SnO in the as-deposited film. Peaks of (101), (110), (200), (112), and (211) directions of α-SnO (α-PbO structure) were detected after the films were annealed. Peaks of Sn were also detected in the annealed films. Sn_3O_4 which is an intermediate oxidation state and can be easily further oxidized to SnO_2 by annealing[21] was detected after the film was annealed at 225 °C. The disappearance of such Sn_3O_4 peak after the film was annealed at 250 °C indicates the formation of SnO_2. SnO_2 is not expected to be shown in the XRD spectra because it is expected to be amorphous at the annealing temperatures in this work.[22,23]

Figure 3 shows the surface morphologies of the 27-nm-thick SnO_x thin films annealed at various temperatures. The as-deposited film was relatively homogeneous and smooth as shown in Fig. 3(a). For the film annealed at 150 °C, feather-like and bright regions (marked by white circle in Fig. 3(b)) were observed and some tiny microgrooves (black region) appeared simultaneously possibly due to formation of polycrystalline of SnO. As the annealing temperature went higher, such feather-like, bright regions and black microgrooves became more obvious (Fig. 3(c)), and needle-like grains started to grow along the microgrooves when

the film was annealed at temperatures above 162 ^{o}C. XRD patterns in Fig. 2 show the crystallization of SnO and metallic Sn in the annealed films. The dominated and continuous composition in films annealed at and above 175 ^{o}C should be SnO due to the observed ambipolar and p-type conduction of TFTs (Fig. 1(b)).

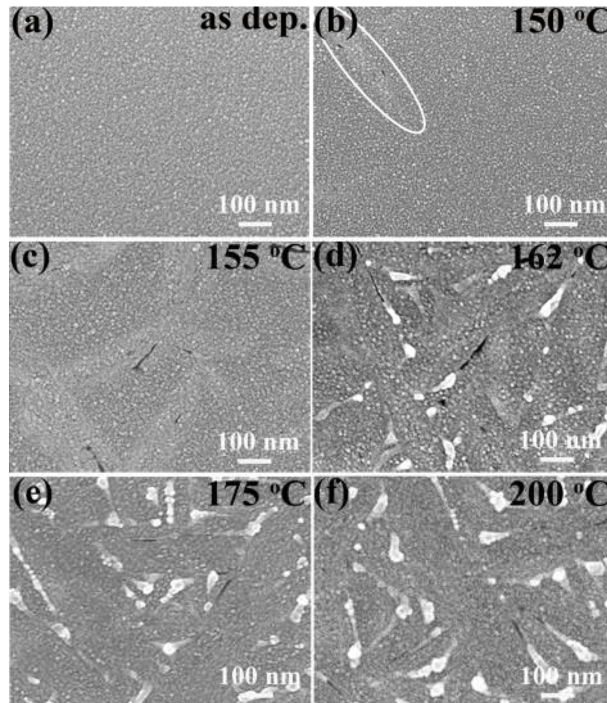

FIG. 3. SEM images of (a) as-deposited SnO_x film, and SnO_x films annealed at (b) 150, (c) 155, (d) 162, (e) 175, and (f) 200 ^{o}C.

Atomic-force-microscopy (AFM) images were taken to study the surface roughness of the films annealed at different temperatures. Figures 4(a) and 4(b) show AFM images of the as-deposited film and film annealed at 200 ^{o}C, respectively. Figure 4(c) shows how the root-mean-square (RMS) roughness changes with the annealing temperature. The RMS roughness of the film shows a sharp increase from 0.60 to 3.73 nm when the film was annealed from 150 to 175 ^{o}C. The drastic change of roughness correlates with the significantly improved transistor on/off ratio at similar annealing temperatures as in Fig. 1(b).

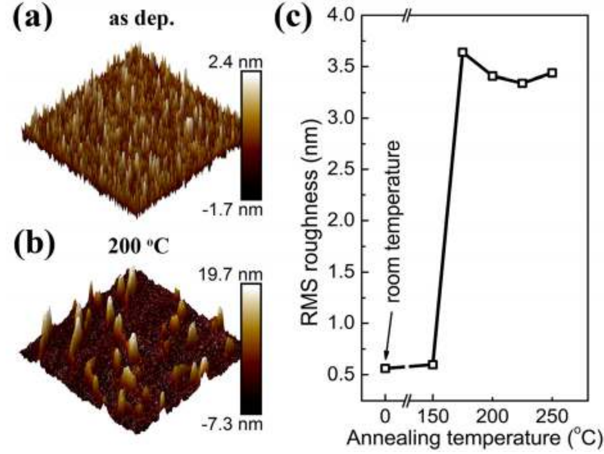

FIG. 4. AFM images of (a) as-deposited SnO_x film and (b) film annealed at 200 ^oC. The scanning size of the AFM images is 1μm × 1μm. (c) Root-mean-square (RMS) roughness of the films as a function of annealing temperature.

To study the nature of the clusters shown in Figs. 3 and 4, we note that previous studies showed that Sn atoms tend to precipitate to the dislocations and grain boundaries and then form Sn quantum dots in the Sn-rich SiO_2 films during annealing.[24] Lei *et al.*[25] also reported a void-mediated formation of Sn quantum dots in a Si matrix. In their studies, voids below Si surface were induced by the lattice mismatch strain and Sn atoms were found to diffuse into these voids. The phenomenon in our experiment may be quite similar to these experiments. In our case, the microgrooves appeared when grain boundaries of polycrystalline SnO was formed when the films were annealed at 175 ^oC as confirmed by XRD.[26] As such, the microgrooves could well be the grain boundaries of polycrystalline SnO. These microgrooves could act as defects that promote the crystal nucleation of metallic Sn, and the high diffusivity of Sn enabled the Sn crystals to grow along the sidewalls of the microgrooves in the annealed films. Furthermore, metallic Sn nucleated along the sidewalls of the microgrooves is expected to reduce the interfacial trap states at the grain boundaries of polycrystalline SnO. During annealing process at and above 162 ^oC (Figs. 3(d-f)), the original dispersed and continuously spread excess Sn in the as-deposited film quite possibly gathered to form Sn clusters along the microgrooves as in Refs. 24 and 25. The diameters of the clusters are 30 ± 9 nm as estimated by SEM. Indeed, the XRD spectra reveal the formation of polycrystalline Sn at annealing temperatures at and above 175 ^oC. Also, the conductivity of the film dropped dramatically after the film was annealed in agreement with the formation of isolated (and hence not able to contribute to the film

conductivity) Sn clusters. Obviously, the segregation of Sn clusters leads to a drastic reduction of Sn_i in the SnO film. According to the first-principle calculations of native defects in SnO, Sn_i is found to induce a huge amount of defect states in the bandgap of SnO.[27] As such, the reduction of Sn_i due to segregation of Sn at the sidewalls of the microgrooves makes it easier to shift the Fermi level.[6,11] Because the bandgap of SnO is only 0.7 eV, the reduction of subgap states may well enable the ambipolar behavior. Indeed, the TFTs annealed at 175 and 200 °C exhibited improved *SS*, low I_{off}, and ambipolar conduction. The TFT annealed at 225 °C showed much larger I_{off} and D_t than those annealed at 200 °C, and the ambipolar behavior disappeared with the disappearance of n-type conduction. This may be due to the excess trap states caused by the formation of oxidized impurities such as Sn_3O_4 and SnO_2 (Sn_3O_4 was detected by XRD when the TFT was annealed at 225 °C, and Sn_3O_4 can easily transform to SnO_2.). These trap states, including both shallow and deep trap states, make it difficult to shift the Fermi level, and as a result, the ambipolar behavior disappeared. The shallow traps led to the deterioration of μ, *SS*, and high I_{off}. With the annealing temperature increase from 225 °C to 250 °C, both I_{on} and I_{off} significantly decreased, and this should be due to the disproportionation reaction "SnO $\rightarrow$ SnO_2 + Sn" was activated at 250 °C.[23] Consequently, the obviously reduced amount of SnO led to the clear decrease of the hole concentration and drain current.

In conclusion, we have fabricated ambipolar SnO_x TFTs by applying a high sputtering power of 200 W and post-annealing treatments. The ambipolar behavior was studied and discussed in the light of characterisation of the film morphology and composition. The results suggest that segregation of excess Sn on the sidewalls of the microgrooves leads to the reduction of density of subgap trap states by Sn interstitials in SnO, making it possible to shift the Fermi level effectively by the gate voltage. As the ambipolar oxide TFT is highly attractive for CMOS-like applications, our results may have useful implications in achieving and optimizing ambipolar behavior in SnO_x films for thin-film-based circuits. In addition, the optimum processing temperature for the ambipolar SnO_x TFT is below 200 °C, so that the results are relevant to possible applications on flexible substrates such as polyimide.

This work was financed by the National Key Research and Development Program of China (Grant No. 2016YFA0301200 and 2016YFA0201800), the National Natural Science

Foundation of China (Grant Nos. 11374185), Engineering and Physical Sciences Research Council (EPSRC) (Grant No. EP/N021258/1), China Postdoctoral Science Foundation funded project (2016M590634), the Key Research and Development Program of Shandong Province (2017GGX10111 and 2017GGX10121), the Natural Science Foundation of Jiangsu Province (BK20151255), Suzhou Planning Projects of Science and Technology (SYG201527 and SYG201616), and the Fundamental Research Fund of Shandong University (2016WLJH44).

[1]Kim Kyung Min, Kim Chi Wan, Heo Jae-Seok, Na Hyungil, Lee Jung Eun, Park Chang Bum, Bae Jong-Uk, Kim Chang-Dong, Jun Myungchul, Hwang Yong Kee, S. T. Meyers, A. Grenville, and D. A. Keszler, Appl. Phys. Lett. **99** (24), 242109 (2011).

[2]Binn Kim, Hyung Nyuck Cho, Woo Seok Choi, Seung-Hee Kuk, Yong Ho Jang, Juhn-Suk Yoo, Soo Young Yoon, Myungchul Jun, Yong-Kee Hwang, and Min-Koo Han, IEEE Electron Device Lett. **33** (4), 528 (2012).

[3]E. Fortunato, P. Barquinha, and R. Martins, Adv. Mater. **24** (22), 2945 (2012).

[4]J. Zhang, Y. Li, B. Zhang, H. Wang, Q. Xin, and A. Song, Nat. Commun. **6**, 7561 (2015).

[5]L. Y. Liang, H. T. Cao, X. B. Chen, Z. M. Liu, F. Zhuge, H. Luo, J. Li, Y. C. Lu, and W. Lu, Appl. Phys. Lett. **100** (26), 263502 (2012).

[6]H. Luo, L. Liang, H. Cao, M. Dai, Y. Lu, and M. Wang, ACS Appl. Mater. Interfaces **7** (31), 17023 (2015).

[7]H. Luo, L. Y. Liang, Q. Liu, and H. T. Cao, ECS J. Solid State Sci. Technol. **3** (9), Q3091 (2014).

[8]E. J. Meijer, D. M. de Leeuw, S. Setayesh, E. van Veenendaal, B. H. Huisman, P. W. Blom, J. C. Hummelen, U. Scherf, J. Kadam, and T. M. Klapwijk, Nat. Mater. **2** (10), 678 (2003).

[9]S. Z. Bisri, C. Piliego, J. Gao, and M. A. Loi, Adv. Mater. **26** (8), 1176 (2014).

[10]Anand Subramaniam, Kurtis D. Cantley, Harvey J. Stiegler, Richard A. Chapman, and Eric M. Vogel, IEEE Trans. Electron Devices **59** (2), 359 (2012).

[11]K. Nomura, T. Kamiya, and H. Hosono, Adv. Mater. **23** (30), 3431 (2011).

[12]Z. Wang, P. K. Nayak, J. A. Caraveo-Frescas, and H. N. Alshareef, Adv. Mater. **28** (20), 3831 (2016).

[13]Toshio Kamiya, Kenji Nomura, and Hideo Hosono, Sci. Technol. Adv. Mater. **11** (4), 044305 (2010).

[14]Yoichi Ogo, Hidenori Hiramatsu, Kenji Nomura, Hiroshi Yanagi, Toshio Kamiya, Mutsumi Kimura, Masahiro Hirano, and Hideo Hosono, Phys. Status Solidi A **206** (9), 2187 (2009).

[15]Jeong Chan-Yong, Lee Daeun, Han Young-Joon, Choi Yong-Jin, and Kwon Hyuck-In, Semicond. Sci. Tech. **30** (8), 085004 (2015).

[16]J. A. Caraveo-Frescas and H. N. Alshareef, Appl. Phys. Lett. **103** (22), 222103 (2013).

[17]Haowei Peng, Andre Bikowski, Andriy Zakutayev, and Stephan Lany, APL Mater. **4** (10), 106103 (2016).

[18]Jiawei Zhang, Xi Kong, Jia Yang, Yunpeng Li, Joshua Wilson, Jie Liu, Qian Xin, Qingpu Wang, and Aimin Song, Appl. Phys. Lett. **108** (26), 263503 (2016).

[19]Po-Chun Chen, Yung-Hsien Wu, Zhi-Wei Zheng, Yu-Chien Chiu, Chun-Hu Cheng, Shiang-Shiou Yen, Hsiao-Hsuan Hsu, and Chun-Yen Chang, J. Disp. Technol. **12** (3), 224 (2016).

[20]Soo Hyun Kim, In-Hwan Baek, Da Hye Kim, Jung Joon Pyeon, Taek-Mo Chung, Seung-Hyub Baek, Jin-Sang Kim, Jeong Hwan Han, and Seong Keun Kim, J. Mater. Chem. C **5** (12), 3139 (2017).

[21]F. Lawson, Nature **215** (5104), 955 (1967).

[22]R. Zenkyu, D. Tajima, and J. Yuhara, J. Appl. Phys. **111** (6), 064907 (2012).

[23]Hao Luo, Ling Yan Liang, Hong Tao Cao, Zhi Min Liu, and Fei Zhuge, ACS Appl. Mater. Interfaces **4** (10), 5673 (2012).

[24]S. Huang, E. C. Cho, G. Conibeer, M. A. Green, D. Bellet, E. Bellet-Amalric, and S. Y. Cheng, J. Appl. Phys. **102** (11), 6 (2007).
[25]Y. Lei, P. Mock, T. Topuria, N. D. Browning, R. Ragan, K. S. Min, and H. A. Atwater, Appl. Phys. Lett. **82** (24), 4262 (2003).
[26]Y. H. Jiang, I. C. Chiu, P. K. Kao, J. C. He, Y. H. Wu, Y. J. Yang, C. C. Hsu, I. C. Cheng, and J. Z. Chen, Appl. Surf. Sci. **327**358 (2015).
[27]A. Togo, F. Oba, I. Tanaka, and K. Tatsumi, Phys. Rev. B **74** (19), 195128 (2006).